2026 Korea Nuclear Society Autumn

Depth-Resolved Viscous Entropy Generation in a Semi-Circular Zigzag PCHE Measured by Refractive-Index-Matched PIV

Gyeongju Hwabaek International Convention Center, Room 201

2026. 10. 29. Thu.

Hyukjoon Lee[1], Sijun Kim[1], Sangoh Shin[1], Minseop Song[1,*] (HYU)

[1]Department of Nuclear Engineering, Hanyang University, 222 Wangsimni-ro, Seongdong-gu, Seoul 04763, Korea

[*]Corresponding author: hysms@hanyang.ac.kr

CONTENTS

1. **Introduction**
2. **Experimental Method**
3. **Results**
    1) Mean and instantaneous velocity fields
    2) Depth dependence and reverse-flow vector fraction
    3) Vorticity and mean in-plane viscous dissipation
4. **Conclusions**

Introduction

The Position of SMRs in the Current Era

- **Surging power demand driven by rapid AI development highlights the importance of SMRs**
- **SMRs are being developed in various designs and operating ranges to maximize their efficiency**
  - Major candidates: MSR, VHTR, and helium / sCO2 power cycles
- **Consequently, operation under more extreme conditions is required**
  - Heat exchangers are also being designed to align with this trend

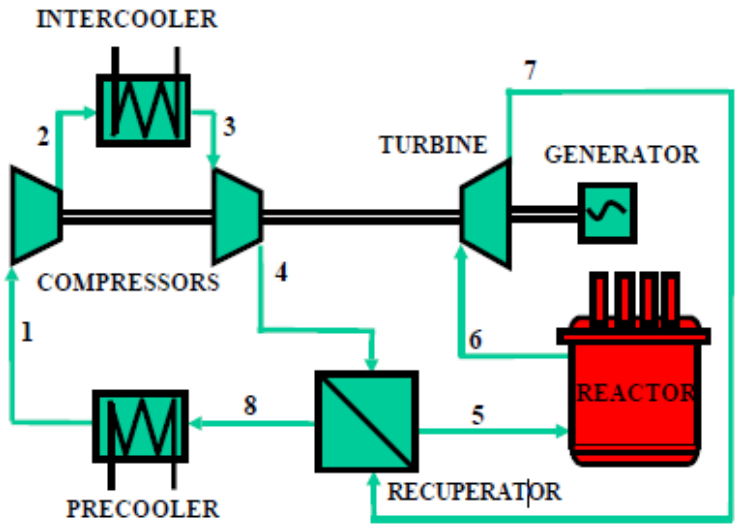


Fig. Supercritical CO_2 recompression Brayton cycle [1]

1. Dostal, V., Driscoll, M. J., Hejzlar, P., & Todreas, N. E. (2002). A supercritical CO2 gas turbine power cycle for next-generation nuclear reactors. In Proceedings of the 10th International Conference on Nuclear Engineering (ICONE10) (Paper No. ICONE10-22192).

Why Use a Printed Circuit Heat Exchanger?

- **A PCHE is a heat exchanger that can maintain its structural integrity under extreme conditions [1]**
  - It uses diffusion bonding to join chemically etched plates into a solid block
  - Temperature up to 900 °C
  - Pressure up to 60 MPa
  - Surface area density above 2,500 m^2/m^3

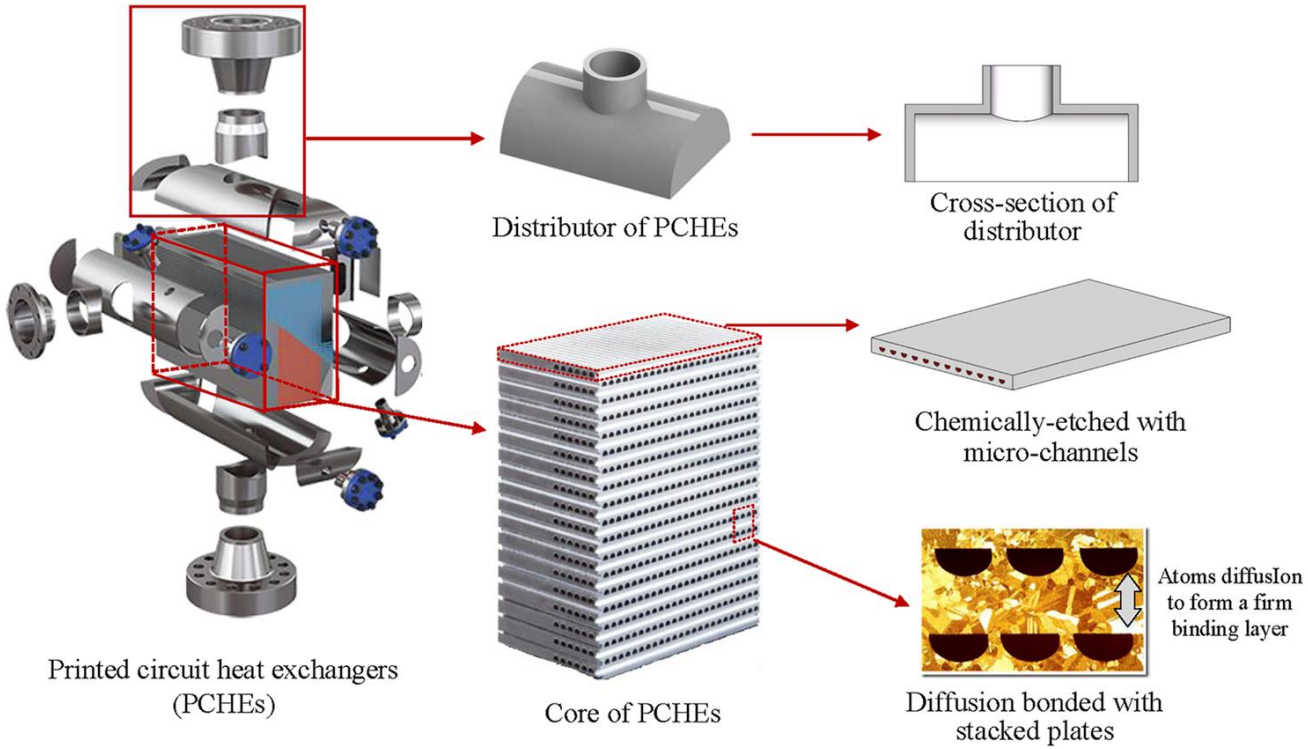


Fig. Structural configuration and diffusion bonding mechanism of PCHE [2]

1. Weng, Y., Tian, K., Yang, Z., & Yang, Z. (2025). Research progress on Printed Circuit Heat Exchangers (PCHEs). Scientific Journal of Technology, 7(9).
2. Xie, L., Zhuang, D., Li, Z., & Ding, G. (2022). Technical characteristics and development trend of Printed Circuit Heat Exchanger applied in floating liquefied natural gas. Frontiers in Energy Research, 10, Article 885607.

PCHE Applications in Nuclear Systems

- **International [1,2]**
  - VHTR and microreactor designs consider a PCHE as the heat exchanger between the reactor and the power cycle
- **Domestic [3,4]**
  - KAERI and KAIST tested PCHEs in high-temperature helium loops for the VHTR IHX
- **Most applications remain at the design and test loop stage**

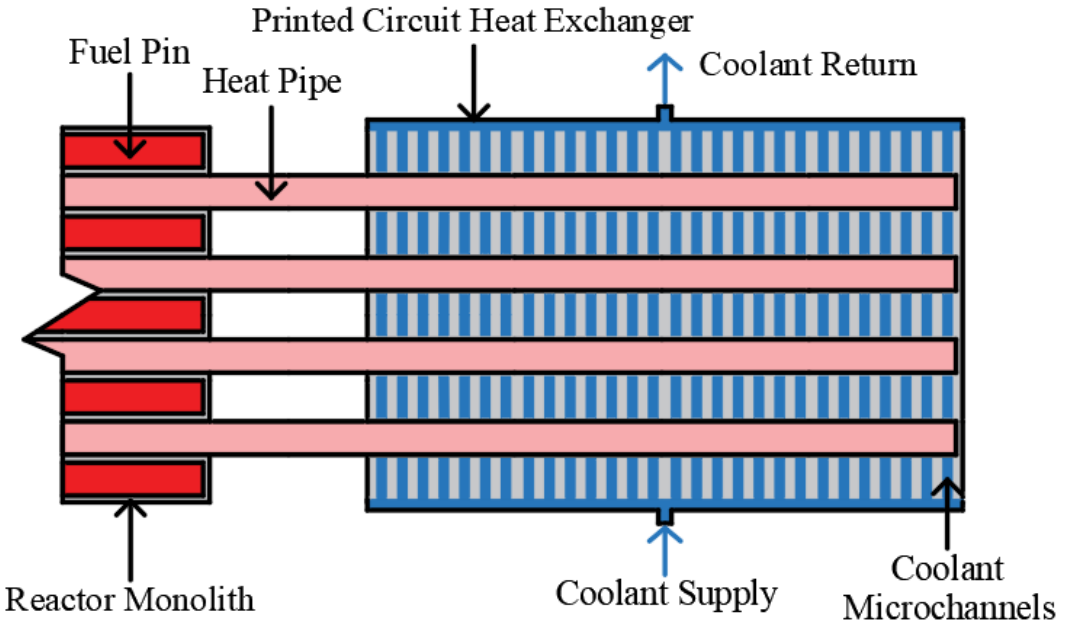


Fig. PCHE coupled to the heat pipes of a microreactor [2]

1. Chen, M., Sun, X., Christensen, R. N., Skavdahl, I., Utgikar, V., & Sabharwall, P. (2016). Pressure drop and heat transfer characteristics of a high-temperature printed circuit heat exchanger. Applied Thermal Engineering, 108, 1409–1417.
2. Foster, C. H., Moreira, T. A., Nellis, G. F., & Anderson, M. H. (2026). Thermohydraulic performance of a supercritical CO2 PCHE for heat pipe microreactors. The 9th International Supercritical CO2 Energy Technologies Symposium, Pittsburgh, PA.
3. Kim, C. S., Hong, S.-D., Kim, E.-S., & Kim, M. H. (2015). High temperature operational experiences of Helium Experimental Loop. Transactions of the Korean Nuclear Society Spring Meeting, Jeju, Korea.
4. Kim, I. H., No, H. C., Lee, J. I., & Jeon, B. G. (2009). Thermal hydraulic performance analysis of the printed circuit heat exchanger using a helium test facility and CFD simulations. Nuclear Engineering and Design, 239(11), 2399–2408.

Representative PCHE channels

- **Semi-circular Channel**
  - Chemical etching facilitates the fabrication of semi-circular channels

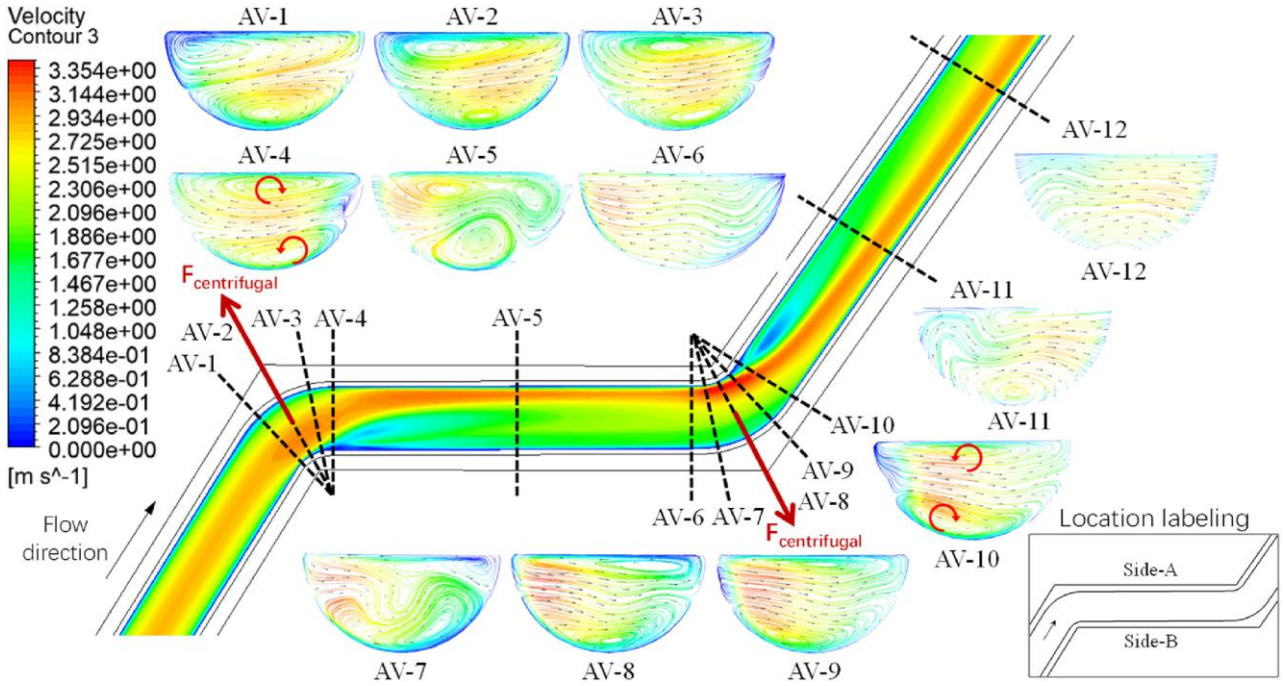


Fig. CFD velocity contours and cross-sectional streamlines in a semi-circular zigzag channel at Re = 2,500 (bend angle 30°, 10 mm between adjacent bends) [1]

- **The Zigzag Channel [1,2]**
  - Bending corners can generate secondary flows and **longitudinal vortices**
  - These characteristics repeat at every bend, affecting the next cycle

1. S.-Q. Chen, S.-H. Liu, D.-L. Wang, H.-J. Wu, R.-H. Zheng, M.-Y. Liu, H.-J. Gong, J.-T. Meng, Y.-P. Huang, X.-L. Zhu, Coupling effects of bend corners with alternating direction on the heat transfer and hydraulic characteristics of zigzag-type printed circuit heat exchanger for the next generation nuclear systems, Prog. Nucl. Energy 180 (2025) 105611.
2. Y. Lee, S. Lee, H.B. Park, K. Seo, W.-T. Hsu, H. Moon, H.T. Nam, S. Lee, H.H. Cho, D. Lee, PIV visualization and CFD analysis of thermal-hydraulic performance in printed circuit heat exchangers with zigzag channels, Case Stud. Therm. Eng. 73 (2025) 106446.

Introduction

Representative PCHE channels

- **The Zigzag Channel [1,2]**
  - Fluid separation and transverse vortices significantly increase the frictional pressure drop
  - However, such features can enhance heat transfer depending on the geometry and flow conditions

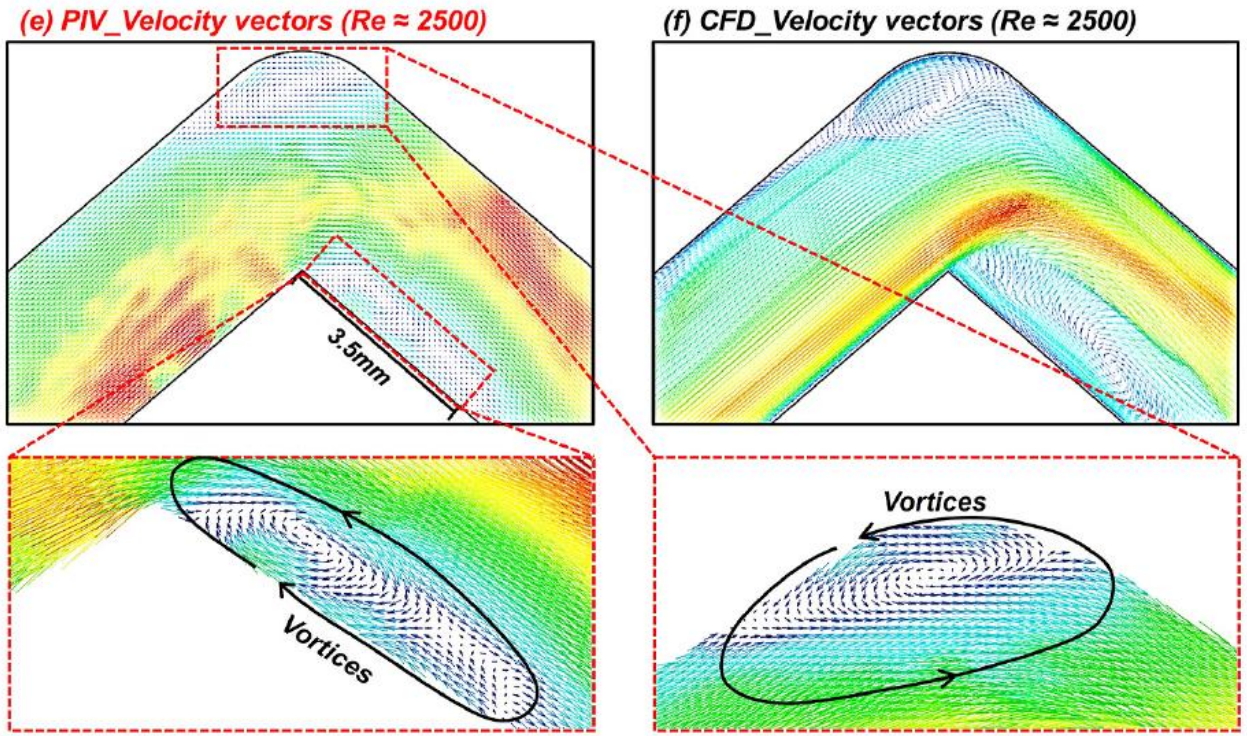


Fig. Velocity contours for a semi-circular zigzag channel from PIV and CFD at Re=2,500 [2]

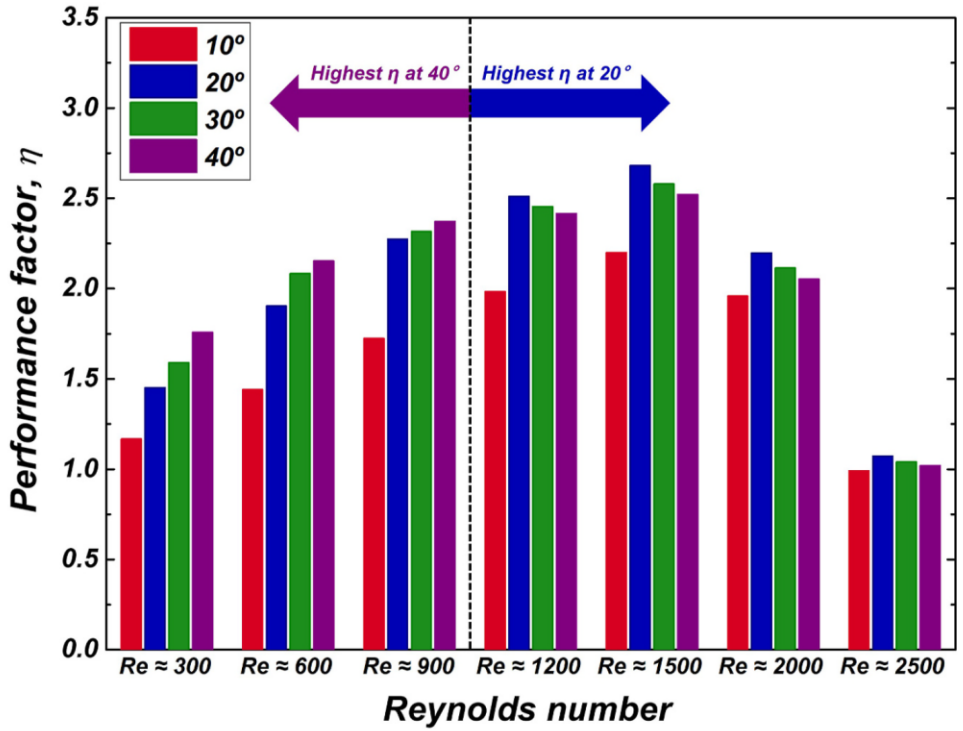


Fig. Performance factors for all geometries under all conditions [2]

1. S.-Q. Chen, S.-H. Liu, D.-L. Wang, H.-J. Wu, R.-H. Zheng, M.-Y. Liu, H.-J. Gong, J.-T. Meng, Y.-P. Huang, X.-L. Zhu, Coupling effects of bend corners with alternating direction on the heat transfer and hydraulic characteristics of zigzag-type printed circuit heat exchanger for the next generation nuclear systems, Prog. Nucl. Energy 180 (2025) 105611.
2. Y. Lee, S. Lee, H.B. Park, K. Seo, W.-T. Hsu, H. Moon, H.T. Nam, S. Lee, H.H. Cho, D. Lee, PIV visualization and CFD analysis of thermal-hydraulic performance in printed circuit heat exchangers with zigzag channels, Case Stud. Therm. Eng. 73 (2025) 106446.

Introduction

The Need for Depth-wise Analysis [1,2]

- The PCHE's semi-circular zigzag flow path has a three-dimensional structure
- Transverse and longitudinal vortices coexist in the channel

As a result, a single-plane analysis cannot fully capture this three-dimensional flow dependence

1. S.-Q. Chen, S.-H. Liu, D.-L. Wang, H.-J. Wu, R.-H. Zheng, M.-Y. Liu, H.-J. Gong, J.-T. Meng, Y.-P. Huang, X.-L. Zhu, Coupling effects of bend corners with alternating direction on the heat transfer and hydraulic characteristics of zigzag-type printed circuit heat exchanger for the next generation nuclear systems, Prog. Nucl. Energy 180 (2025) 105611.
2. Y. Lee, S. Lee, H.B. Park, K. Seo, W.-T. Hsu, H. Moon, H.T. Nam, S. Lee, H.H. Cho, D. Lee, PIV visualization and CFD analysis of thermal-hydraulic performance in printed circuit heat exchangers with zigzag channels, Case Stud. Therm. Eng. 73 (2025) 106446.

Viscous Dissipation and Measurement Scope

- **Viscous dissipation**
  - Velocity gradients convert mechanical energy irreversibly into internal energy
- **Measurement scope**
  - The present nearly isothermal experiment examines the viscous contribution using the measured mean velocity
  - Only the in-plane gradients of the mean velocity are resolved on each plane

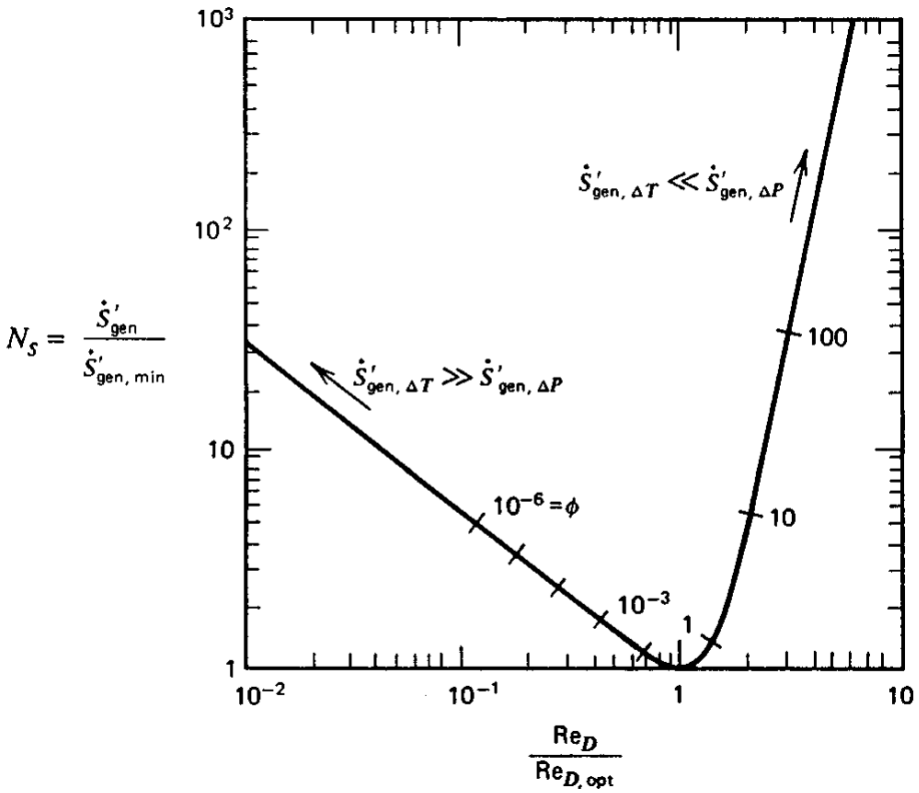


Fig. Relative entropy generation of a smooth tube with heat transfer [1]

1. Bejan, A. (1996). Entropy generation minimization: The new thermodynamics of finite-size devices and finite-time processes. Journal of Applied Physics, 79(3), 1191–1218.

Introduction

Research Objectives

- Compare three depths under three flow conditions using refractive-index-matched PIV
- Quantify depth variation using the reverse-flow vector fraction
- Locate the mean in-plane viscous dissipation relative to the reversed region
- Provide a depth-resolved experimental dataset for future CFD and correlation validation

Experimental Method

Test Section and Flow Loop Setup

- **Transparent test section**
  - A single semi-circular zigzag PCHE channel, **enlarged** and printed by stereolithography in Clear V5 resin
  - Semi-circle with R **= 15 mm, pitch 120 mm,** each segment inclined 20° to the mean flow (40° turn at every corner)
- **Closed loop**
  - Inverter-controlled pump, in-line heat exchanger within 0.2 °C per run, K-type thermocouple, clamp-on flowmeter

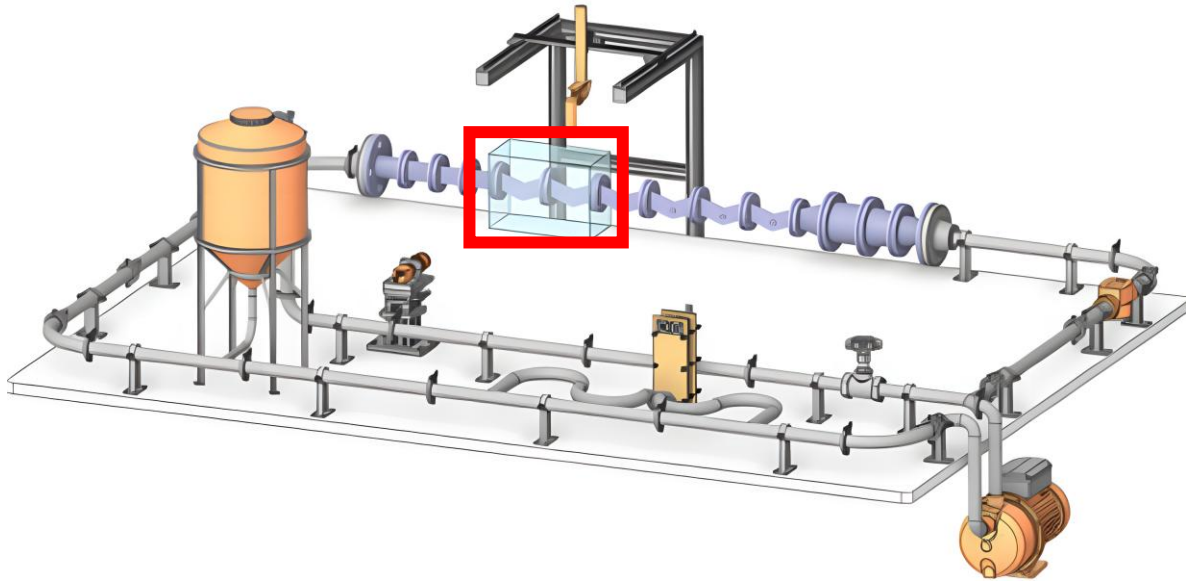


Fig. Closed flow loop with the transparent test section at the center

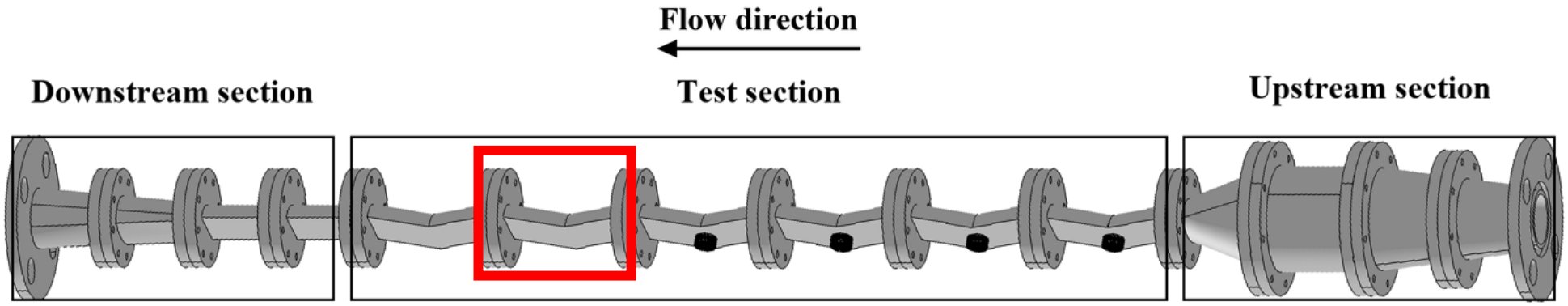


Fig. CAD model of the channel as assembled for the experiment, flow from right to left

Experimental Method

Refractive Index Matching

- **Refractive-index-matched (RIM) fluid**
  - Complex, curved geometries cause light refraction and optical aberration
  - Using a RIM fluid minimizes optical distortion
  - Benzyl benzoate and isopropyl myristate at 84:16, n = 1.546 as the resin [1]



Fig. 3D-printed test section in air (top) and in the index-matched solution (bottom)

1. Shin, S., & Song, M. (2026). Experimental validation of a novel refractive index matching technique using SLA 3D-printed models for optical flow measurements in nuclear thermal-hydraulic experiments. Transactions of the American Nuclear Society, 2026 ANS Annual Conference, Denver, CO.

Experimental Method

PIV Calculation Settings

- **Planar two-component PIV**
  - Nd:YAG laser, 532 nm and 200 mJ per pulse, Rhodamine B tracers of 15 µm with 580 nm emission
  - CCD camera 2756 × 2208 px with a 100 mm lens
- **Vector processing**
  - 32 × 32 px window at 50 % overlap
  - One mask per case removes about one vector pitch at each wall
- **Tracer fidelity**
  - Tracer fidelity was assessed using a local maximum velocity, yielding St from $\mathbf{5.8\times10^{-4}}$ to $\mathbf{1.2\times10^{-3}}$

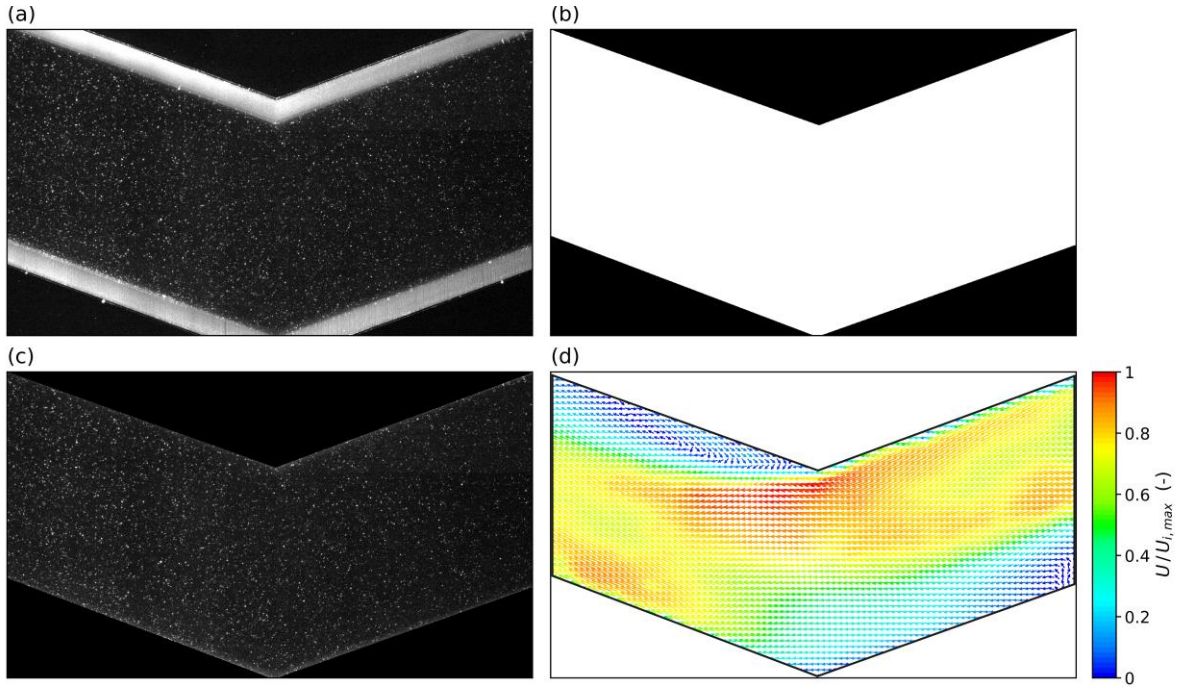


Fig. One image pair through the vector computation at Re 7,043 on P1, (a) second frame, (b) mask, (c) masked image, (d) velocity field averaged over 312 pairs

Major Parameter Definitions

Normalized Viscous Dissipation [1, 2]

- The measurement is nearly isothermal, so only the viscous term of Eq. (1) remains
- The normalized viscous dissipation $\dot{S}^*$ is that term multiplied by T and divided by $\rho U_b^3/D_h$, which puts the nine cases on one scale

$$\dot{S}'''_{\text{gen}} = \frac{k(\nabla T)^2}{T^2} + \boxed{\frac{\mu\Phi}{T}} \tag{1}$$

$$\mu\Phi = 2\mu[(\frac{\partial u}{\partial x})^2 + (\frac{\partial v}{\partial y})^2] + \mu(\frac{\partial u}{\partial y} + \frac{\partial v}{\partial x})^2 \tag{2}$$

Normalized Vorticity

- $\frac{\omega_z D_h}{U_b}$ is used to compare cases with different conditions

$$\dot{S}^* = \frac{\mu\Phi D_h}{\rho U_b^3} \tag{3}$$

$$\omega_z = \frac{\partial v}{\partial x} - \frac{\partial u}{\partial y} \tag{4}$$

1. Shi, L., & Ma, H. (2019). Effect of incidence angle on entropy generation in the boundary layers on the blade suction surface in a compressor cascade. Entropy, 21(11), Article 1049. https://doi.org/10.3390/e21111049
2. Bejan, A. (1996). Entropy generation minimization: The new thermodynamics of finite-size devices and finite-time processes. Journal of Applied Physics, 79(3), 1191–1218.

Measurement Setup

- **Nine cases on the same bend**
  - P1 to P3 at z = 12, 10 and 8 mm from the bottom of the cross-section (z/D_h = 0.655, 0.546 and 0.436)
  - Three bulk Re on each plane, 312 image pairs per case

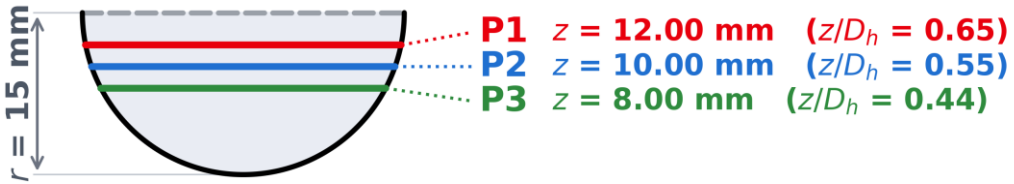


Fig. Positions of the three planes within the channel cross-section

	***Re* 7,043**	***Re* 10,107**	***Re* 13,347**
***Re* (range)**	7,031~7,055	10,039~10,176	13,303~13,392
***Q* (L/min)**	50.2~50.7	69.7~70.4	86.2~86.8
U_b **(m/s)**	2.377~2.379	3.301~3.306	4.077~4.079
***T* (°C)**	28.5~28.8	30.1~30.9	34.2~34.7
μ **(cP)**	6.62~6.64	6.37~6.45	5.97~6.01
ρ **(kg/m³)**	1071.08~1071.17	1070.11~1070.43	1068.35~1068.54
Δt **(μs)**	56.6	40.7	33.0
N pairs	312	312	312

Table. Measurement conditions of the nine cases. Q and T span the lowest and the highest readings of the three runs of a group

Experimental Method

Measurement Setup

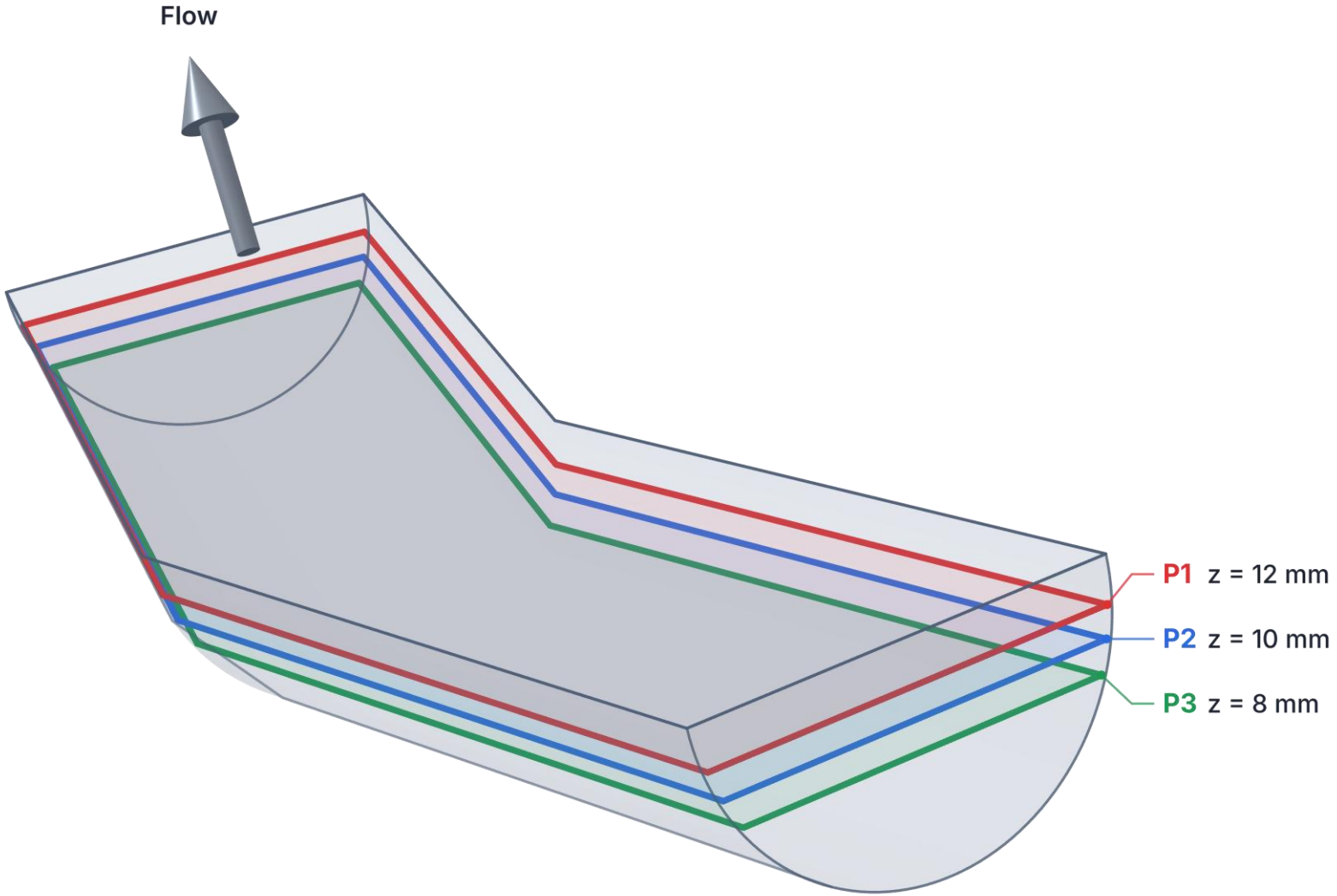
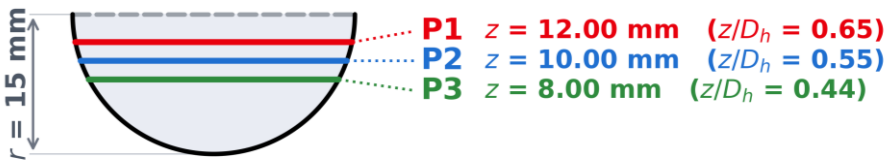


Fig. Positions of the three planes within the channel cross-section in 3D

Results

Mean Velocity Field for All Cases



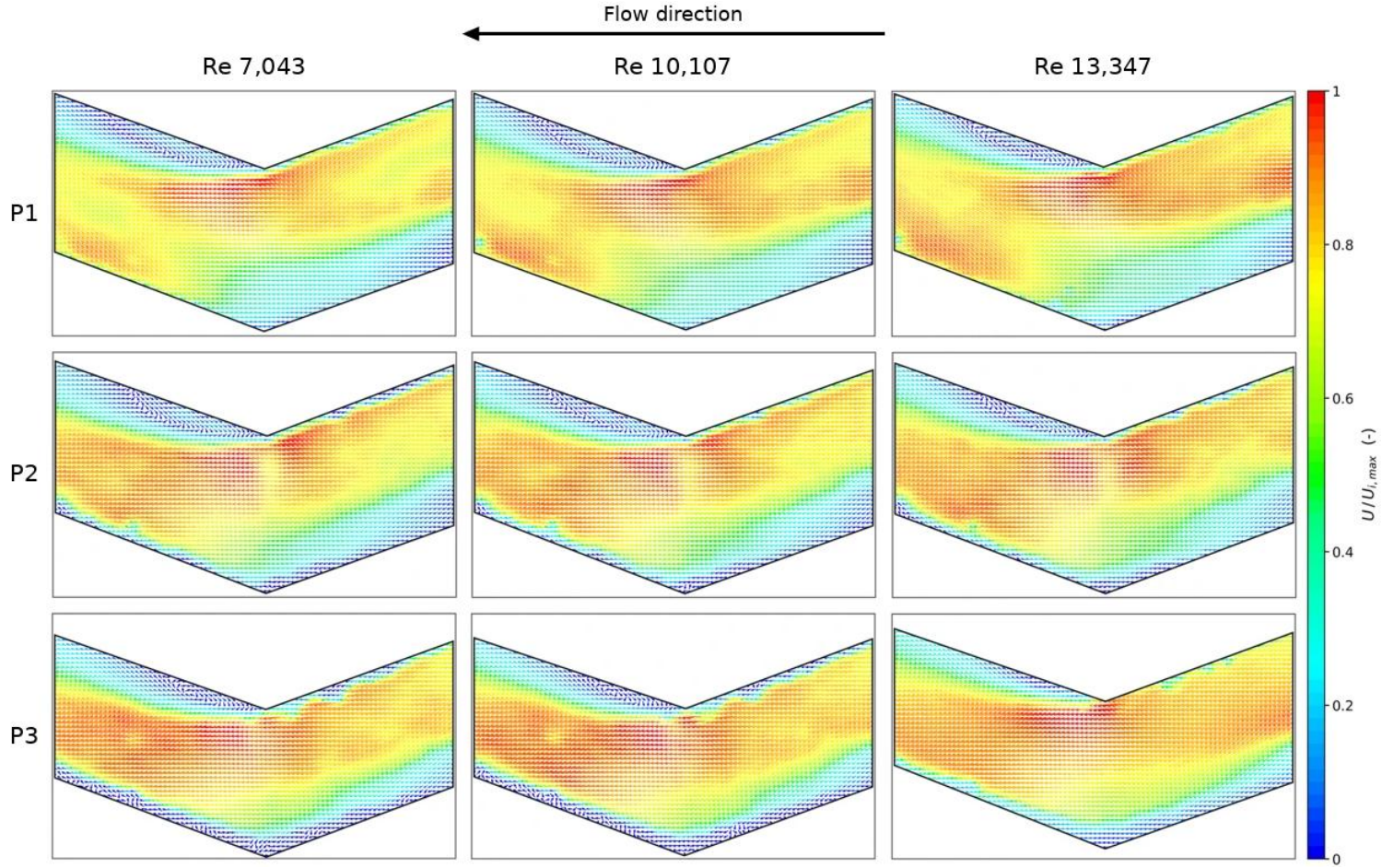
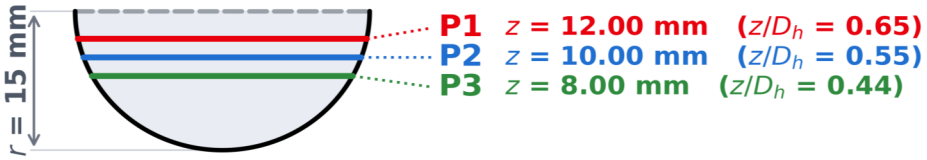


Fig. Time-averaged in-plane velocity vectors of the nine cases, colored by $U/U_{i,max}$. The straight lines are the channel walls fitted to the edge of the mask

Results

Mean Velocity Field in P2, Re = 7,043

- **Two regions are magnified to examine the flow characteristics**
  - (b) shows reversed vectors on the inner wall, below the region where the flow separates at the bend corner
  - (c) shows no reversed vectors on the outer wall around the vertex



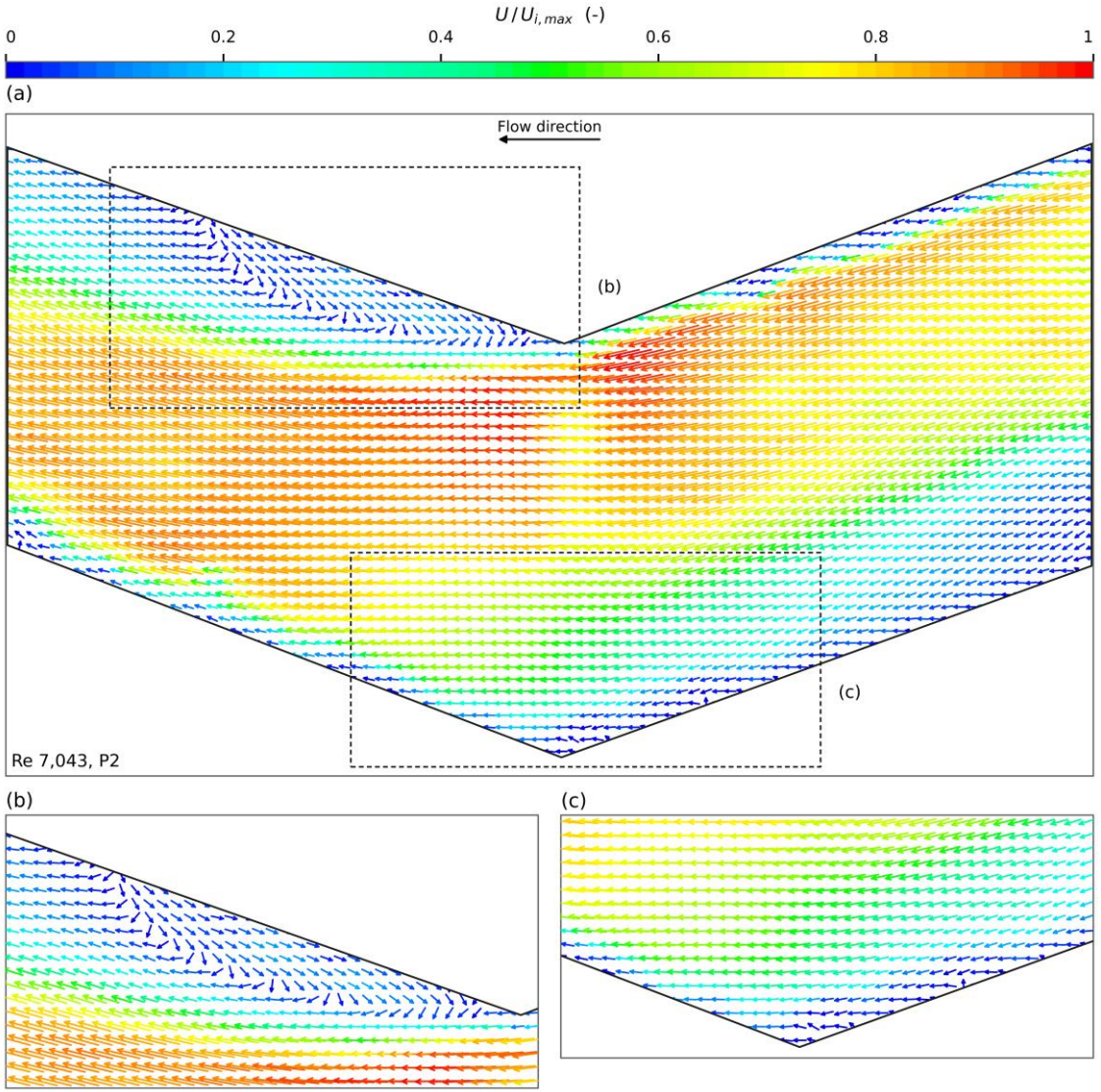
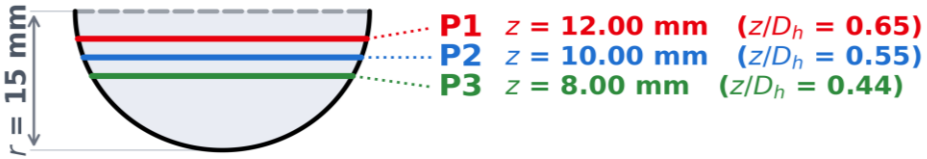


Fig. Time-averaged in-plane velocity vectors on plane P2 at Re 7,043, colored by $U/U_{i,max}$

Results

Mean Velocity Field in P3, Re = 7,043

- **Two regions are magnified to examine the flow characteristics**
  - (b) also shows reversed vectors below the region where the flow separates at the bend corner



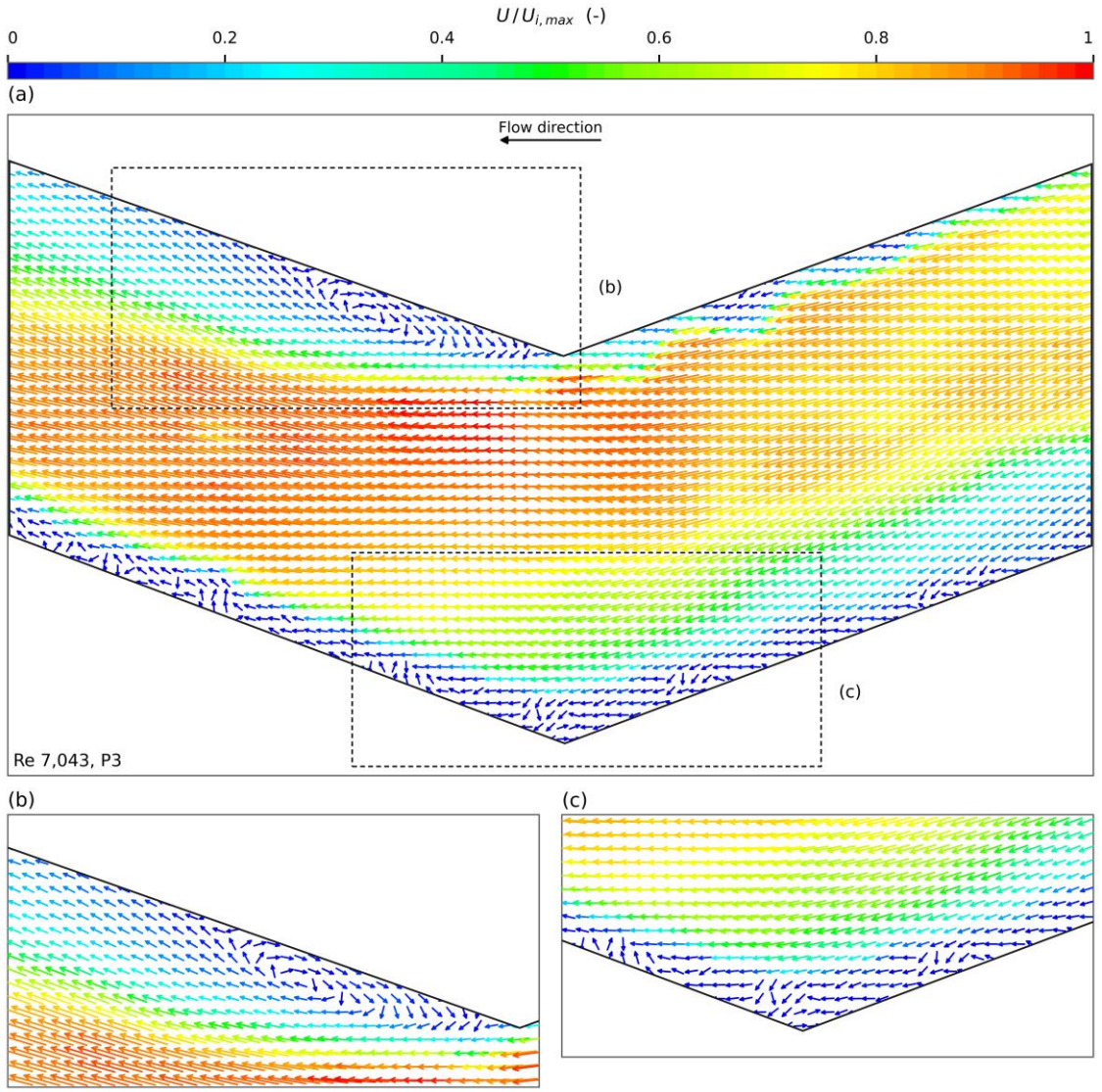
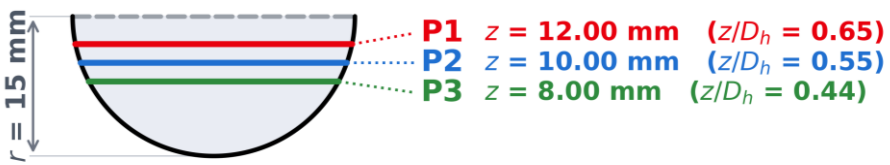


Fig. Time-averaged in-plane velocity vectors on plane P3 at Re 7,043, colored by $U/U_{i,max}$

Results

Instantaneous Velocity Field for All Cases



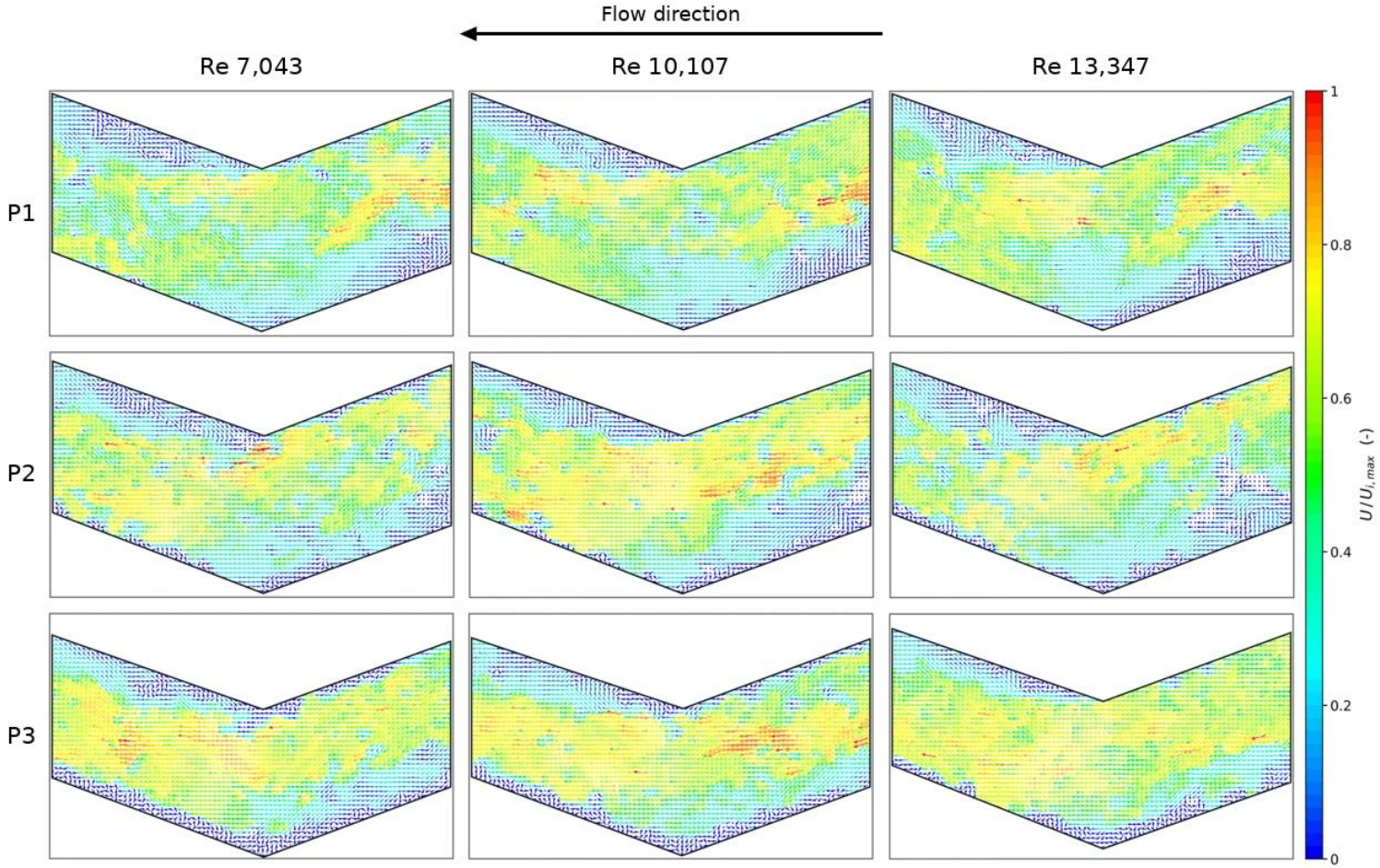


Fig. Instantaneous in-plane velocity vectors of the nine cases, colored by $U/U_{i,max}$. A dot marks each vector of exactly zero displacement

Results

Mean Reverse-Flow Vector Fraction [1,2]

$$f_{rev}(\%) = 100 \times \frac{N_{rev}}{N_{ROI}}$$

- N_{ROI} : **All valid grid points in the common ROI, the streamwise extent shared by the nine measured fields**
- N_{rev} : **Valid grid points with negative mean streamwise velocity**

- **Criterion and precedent**
  - Negative mean streamwise velocity identifies reverse flow within the ROI, and no magnitude threshold is applied here [1,2]

Re	P1	P2	P3
7,043	3.22%	3.10%	1.94%
10,107	2.83%	2.87%	2.33%
13,347	2.07%	2.09%	0.00%

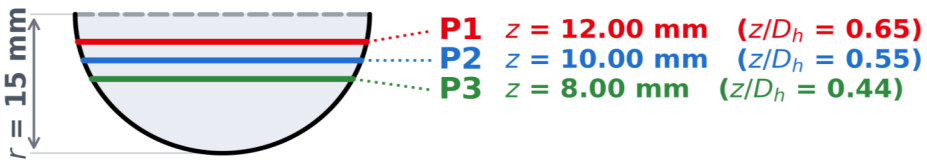
Table. Mean reverse-flow vector fraction (%) within the common ROI

1. Bekhradinasab, A., Al-Zaili, J., & Vakilipour, S. (2021). Large eddy simulation of separated flow to investigate heat transfer characteristics in an asymmetric diffuser subjected to constant wall heat flux. International Communications in Heat and Mass Transfer, 128, Article 105634.
2. Cherry, E. M., Elkins, C. J., & Eaton, J. K. (2008). Geometric sensitivity of three-dimensional separated flows. International Journal of Heat and Fluid Flow, 29(3), 803–811.

Results

Depth Trend in Mean Reverse-Flow Vector Fraction

- **Depth dependence**
  - P3 has the lowest fraction at each Reynolds number
  - P1 and P2 show similar fractions with no consistent ordering
- **Reynolds number dependence**
  - P1 and P2 decrease with increasing Reynolds number
  - On P3, no mean reversal is detected in the ROI at Re = 13,347



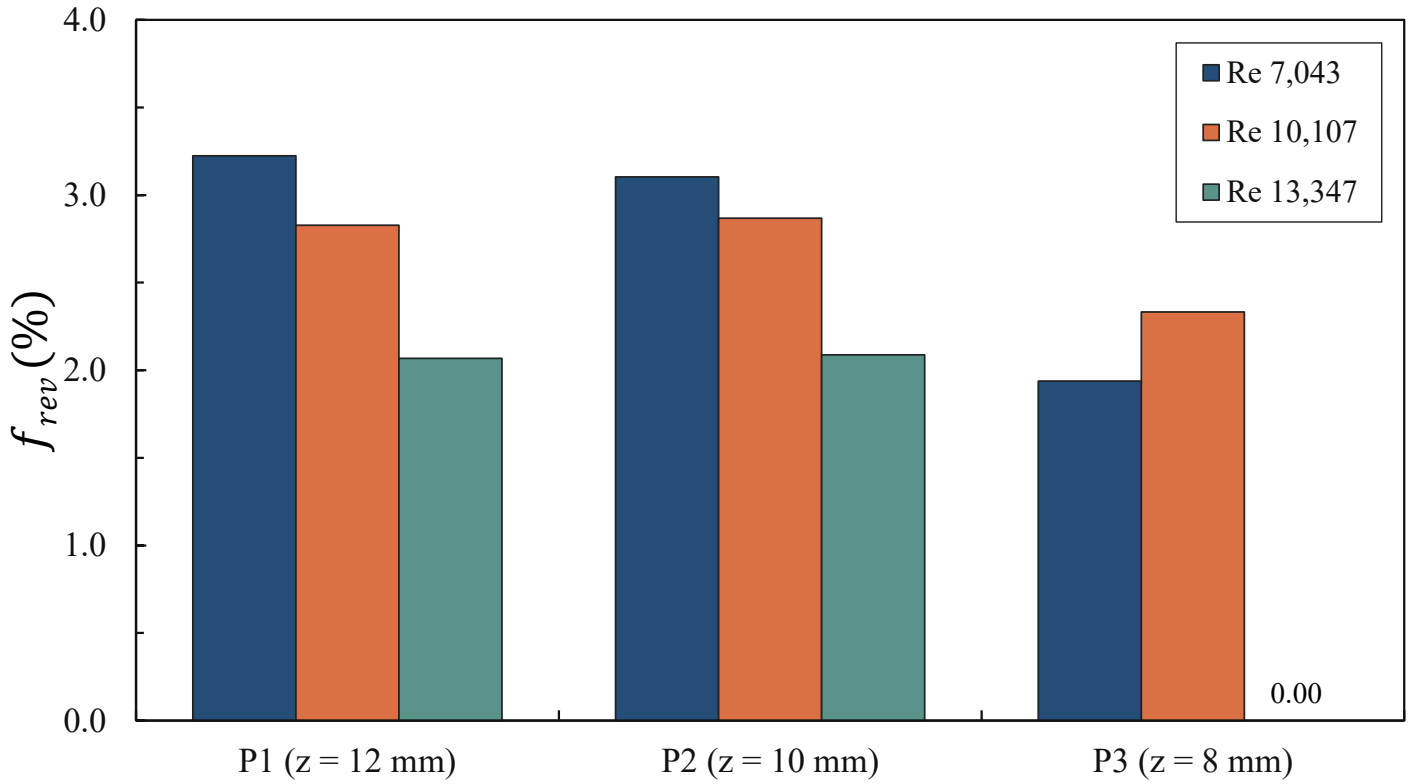
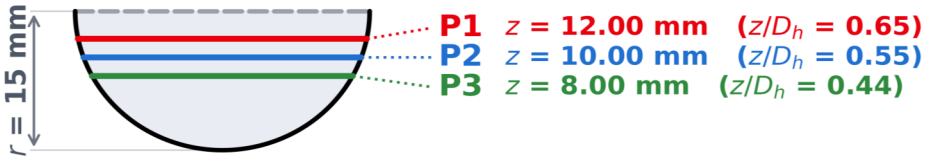


Fig. Mean reverse-flow vector fraction within the common ROI. Near-zero signs, wall masking and vector processing affect the detected fraction [1,2,3]

1. Bekhradinasab, A., Al-Zaili, J., & Vakilipour, S. (2021). Large eddy simulation of separated flow to investigate heat transfer characteristics in an asymmetric diffuser subjected to constant wall heat flux. International Communications in Heat and Mass Transfer, 128, Article 105634.
2. Cherry, E. M., Elkins, C. J., & Eaton, J. K. (2008). Geometric sensitivity of three-dimensional separated flows. International Journal of Heat and Fluid Flow, 29(3), 803–811.
3. Coletti, F., Verstraete, T., Vanderwielen, T., Bulle, J., & Arts, T. (2011). Optimization of a U-bend for minimal pressure loss in internal cooling channels—Part II: Experimental validation. In ASME 2011 Turbo Expo: Turbine Technical Conference and Exposition (Vol. 5: Heat transfer, Parts A and B, pp. 1689–1699). American Society of Mechanical Engineers.

Vorticity and the Separated Shear Layer

- **Inner-wall shear layer**
  - Negative vorticity follows the attached layer into the separated layer
- **Other resolved layers**
  - The outer-wall layer has the opposite vorticity sign
  - A further band enters the upstream outer half



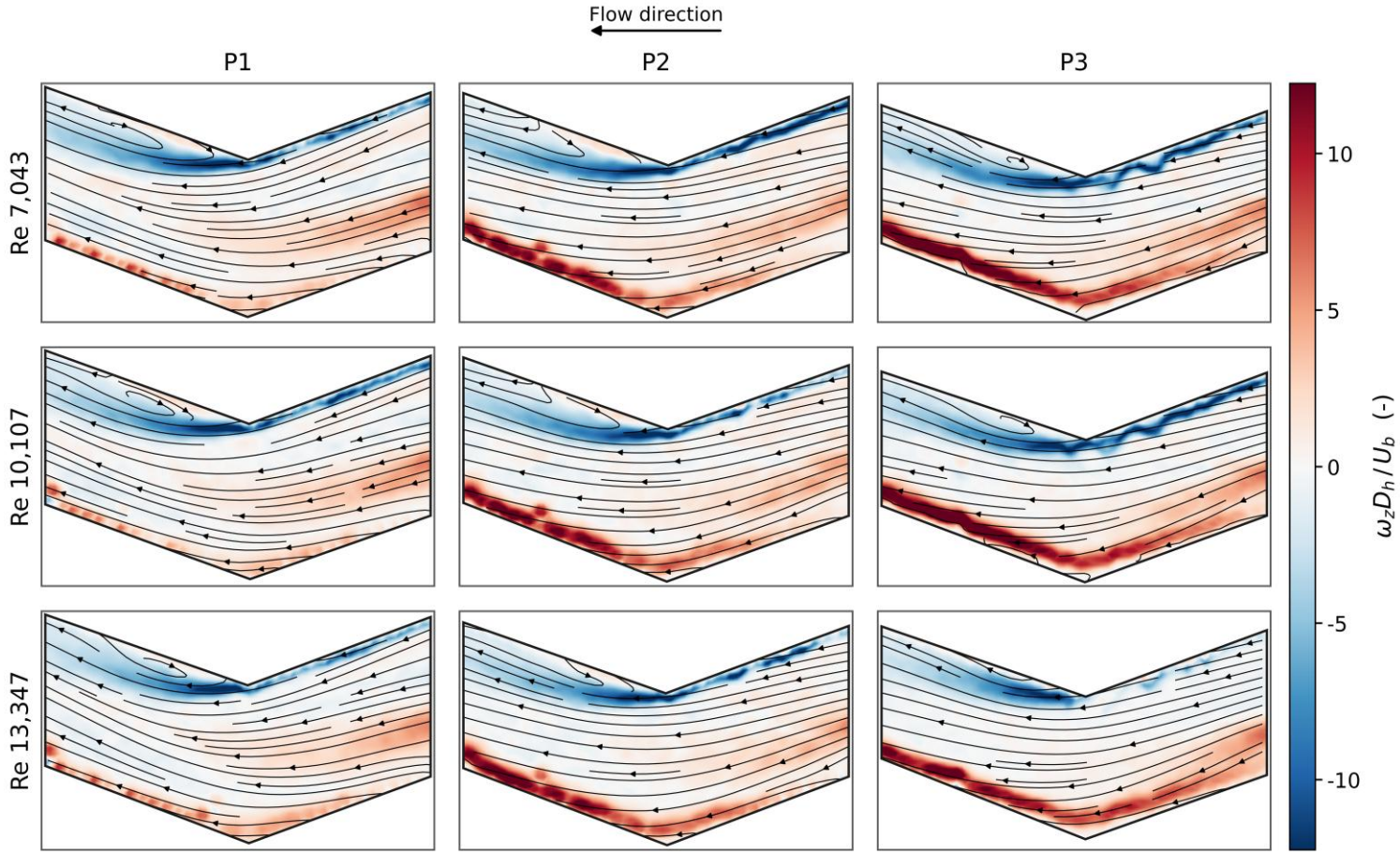
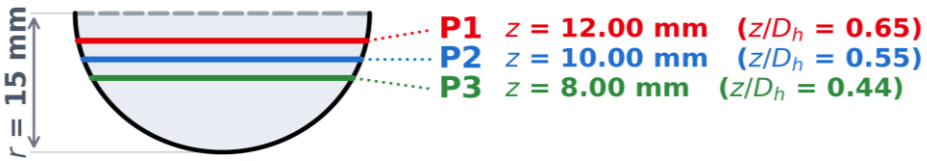


Fig. Normalized mean in-plane vorticity with streamlines of the measured mean field. Positive values indicate counterclockwise rotation as drawn

Mean In-Plane Viscous Dissipation

- **Resolved mean-field contribution**
  - Bright regions mainly follow the attached inner-wall layer and its separated continuation
  - Additional regions occur at the outer wall and upstream outer half
- **Relation with flow structure**
  - The highest 1 % lies outside the reversed region in every case with reversal



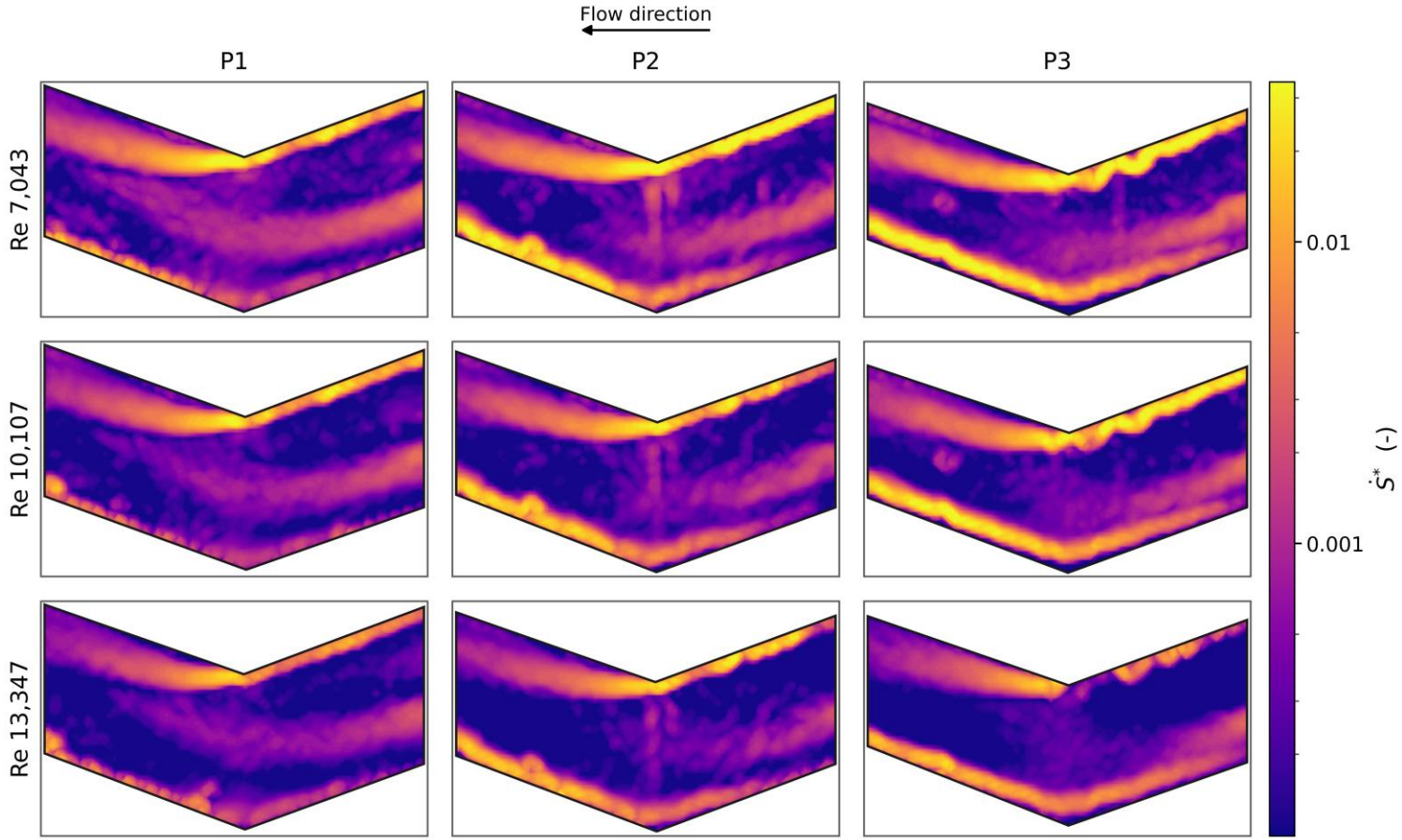
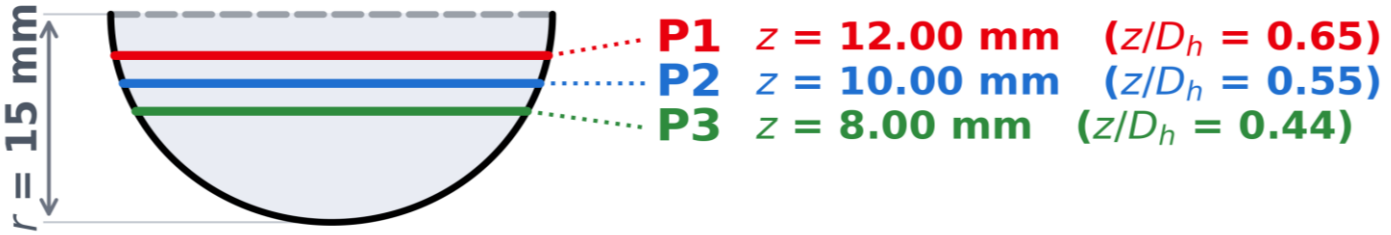


Fig. Resolved mean in-plane dissipation on a common logarithmic scale

Conclusions

Summary

- Flow characteristics of a semi-circular zigzag PCHE were resolved for nine cases using 2D2C RIM-PIV
- P3 has the lowest mean reverse-flow vector fraction at each Reynolds number, while P1 and P2 show similar fractions
- The fraction decreases with Reynolds number on P1 and P2, and P3 shows no mean reversal at Re = 13,347
- The highest resolved mean in-plane dissipation follows the attached inner-wall layer and its separated continuation, outside the reversed region
- Reverse flow changes with depth, so a single plane cannot represent the bend



Thank you for Listening

Hyukjoon Lee
hjune1219@hanyang.ac.kr